RSC Applied Polymers

ROYAL SOCIETY OF CHEMISTRY

PAPER

View Article Online
View Journal | View Issue

Cite this: *RSC Appl. Polym.*, 2025, **3**, 347

Triazolinedione-functionalized isoprene rubber composites with self-adhesion *via* cross-linking with zinc dimethacrylate†

Kyohei Kotani,*[a,b] Yuji Kitamura,[a] Katsuhiko Tsunoda,[a] Akira Takahashi [b] and Hideyuki Otsuka *[b,c]

We report a novel system for the direct adhesion of cross-linked rubbers based on the introduction of triazolinedione (TAD)-derived urazole moieties into *cis*-1,4-polyisoprene (PI) followed by the addition of zinc dimethacrylate (ZDMA) with the aim of forming dissociative ionic cross-links. The modification of PI is achieved by a TAD-based click reaction using 4-phenyl-1,2,4-triazoline-3,5-dione (PhTAD). The formation of cross-linking *via* the TAD units and ZDMA is demonstrated by the increase in the elastic-torque curves of the resulting rubber composites at elevated temperature. The addition of the radical-trapping agent *N*-(1,3-dimethylbutyl)-*N*′-phenyl-*p*-phenylenediamine to the cross-linking system suppresses the increase in its elastic torque, indicating that cross-linking between the TAD units and ZDMA proceeds by a radical mechanism. This mechanism is supported by the fact that the use of either zinc chloride or zinc acetate instead of ZDMA did not show an increase in the elastic torque, excluding the possibility of coordination cross-linking between TAD units and zinc centres. The obtained TAD–ZDMA cross-linked rubbers show unique temperature dependence in dynamic mechanical analysis (DMA), reflecting the dissociation of the ionic cross-linking at elevated temperatures. Strain–sweep DMA tests showed a typical Payne effect with an increasing amount of TAD units in the PI, supporting the formation of ZDMA–ZDMA filler interactions. Tensile tests revealed that the fracture energies of the TAD-PI/ZDMA composites are comparable to those of samples prepared using a peroxide-based curing system, and a tensile strength of up to 18.2 MPa at 525% elongation was achieved when 3.1 mol% of TAD was incorporated into the PI with 40 phr of ZDMA. A direct adhesion is demonstrated using T-peel tests, in which the adhesion-peeling force reached up to 6.55 N mm^{-1} when 4.3 mol% of TAD was incorporated into the PI with 40 phr of ZDMA. The maximum peeling force shows a good correlation with the difference between the *E*′ values at 25 °C and 145 °C in the DMA tests, except in the case of the sample with a too-high degree of cross-linking, indicating that the degree of dissociative cross-linking is the main factor determining the adhesion strength in the TAD–ZDMA cross-linking system.

Received 5th November 2024,
Accepted 26th December 2024

DOI: 10.1039/d4lp00331d

rsc.li/rscapplpolym

Introduction

Adhesion between cross-linked rubbers is an essential process during the production of rubber products such as tyres.[1] However, direct adhesion between cross-linked rubbers without pretreatment of their surfaces is extremely challenging due to the low mobility of polymer chains resulting from the cross-linking.[1–5] Thus, repair processes that involve adhesion between cured cross-linked rubbers, such as tyre retreading, are still limited by factors such as the complexity of the pretreatment process, curing temperature and time.[6–13]

One promising approach to achieve efficient direct adhesion between cross-linked rubbers without pretreatment is the incorporation of dissociative cross-linkages,[1,14–22] such as hydrogen bonds,[23–32] metal–ligand coordination bonds,[25,31,33–45] host–guest interactions,[46,47] dynamic covalent bonds,[48–59] or ionic interactions,[32,60–72] into rubber composites. These linkages usually dissociate at high temperature, endowing the composites with good malleability during conventional hot-pressing adhesion processes. Isoprene rubbers (*cis*-1,4-polyisoprene: PI) including natural rubber (NR) are the

[a]*Sustainable and Advanced Materials Division, Bridgestone Corporation, 3-1-1, Ogawahigashi-cho, Kodaira-shi, Tokyo 187-8531, Japan. E-mail: kyohei.kotani@bridgestone.com*
[b]*Department of Chemical Science and Engineering, Institute of Science Tokyo, 2-12-1 Ookayama, Meguro-ku, Tokyo 152-8550, Japan. E-mail: otsuka@mct.isct.ac.jp*
[c]*Research Center for Autonomous Systems Materialogy (ASMat), Institute of Integrated Research, Institute of Science Tokyo, Japan*

† Electronic supplementary information (ESI) available. See DOI: https://doi.org/10.1039/d4lp00331d

most widely used materials in rubber products,[73] and accordingly, the creation of dissociative cross-linked PI materials has been widely studied.[21–23,25,35,40,45,50,59,62,63,65–67,70,71,74] For example, Chino *et al.* have reported the preparation of functionalized PI through reaction with maleic anhydride (MAH) followed by the addition of 3-amino-1,2,4-triazole; the thus obtained modified PI showed thermo-reversible behaviour due to supramolecular hydrogen-bonding networks.[23] Chen *et al.* have designed a self-healing natural rubber by incorporating a dissociative ionic supramolecular hybrid network, which was created through the *in situ* reaction of methacrylic acid (MAA) and zinc oxide (ZnO) to give zinc dimethacrylate (ZDMA) in NR latex, followed by dicumyl-peroxide (DCP)-induced polymerization of ZDMA.[62] The NR composite with the optimum MAA/ZnO ratio showed excellent self-healing properties through reconstruction of the ionic supramolecular hybrid network and was completely healed after 15 min. Hua *et al.* have reported the use of various approaches to prepare dual ionic cross-linkages in NR. First, the reaction with MAH through an anionic mechanism using *n*-butyllithium was carried out.[65] Subsequently, ZDMA was reacted with the MAH-modified NR using DCP, and the second ionic network was constructed. The resulting dissociative ionic cross-linked NR composites exhibited a high reinforcing effect with a high self-healing efficiency of 75% in full-cut mode.

Additionally, the incorporation of reactive functional groups into the PI backbone is of great interest. One of the most efficient methods for this is click chemistry,[75] which is a high atom-efficiency chemical reaction performed under relatively mild conditions. In particular, triazolinedione (TAD) click chemistry[49,58,76–85] is known to be a powerful tool to incorporate functional groups into PIs. For example, Saville has demonstrated that 4,4′-methylene-bis(1,4-phenylene)-di-1,2,4-triazoline-3,5-dione reacts with NR, resulting in instant gelation due to cross-linking.[77] Guo and Zhang *et al.* have recently used TAD click-chemistry with 4-phenyl-1,2,4-triazoline-3,5-dione (PhTAD) to introduce urazole groups onto NR backbones. The prepared modified NRs showed good carbon black (CB) dispersion capability due to the reaction between the stable urazole radicals on the TAD-modified NR and CB.[85] However, methods for rubber repair or adhesion using PIs modified with filler-reinforced TAD have not yet been developed, because TAD-modified PIs show strong interactions with fillers[85] such as CB, leading to a loss of dissociative cross-linking.

In this study, we investigated the creation of such a system of dissociative cross-linked TAD-modified PIs reinforced by fillers. ZDMA was selected for the formation of ionic dissociative networks with TAD-modified PIs; direct bonding of ZDMA with the TAD-derived urazole group was expected based on the radical-generation capability of the urazole unit.[85–87] ZDMA is widely used in rubber technology as a cross-linking agent and a reinforcing filler.[43,62,64–66,68–70,88–95] Moreover, our group has previously reported direct adhesion between cross-linked rubbers consisting of ZDMA.[43] In our previous study, main-chain-functionalized styrene–butadiene rubbers (SBRs) were used to investigate the direct adhesion performance, and the incorporation of functional groups was achieved through a tetrazine-based click reaction with 3,6-di(2-pyridyl)-1,2,4,5-tetrazine (DPT). However, we found that the tetrazine-based click reaction did not proceed between PIs and DPT. Therefore, an alternative strategy using a TAD-click reaction was selected in the present study. The objective of this study was to design novel cross-linked PI composites that exhibit direct adhesion behaviour without the need for pretreatment (Fig. 1). For this purpose, we prepared a series of PhTAD-modified PI samples using TAD-based click chemistry,[85] before we compounded the obtained TAD-modified PIs with ZDMA. The cross-linking between the TAD units in PI and ZDMA was investigated in

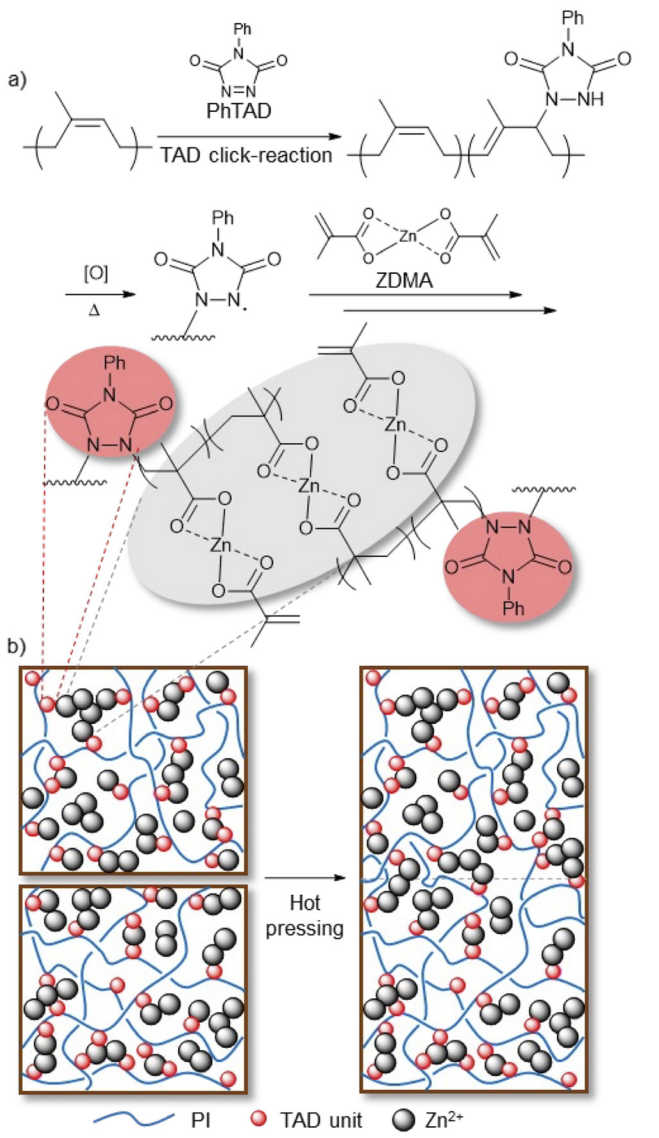

Fig. 1 Conceptual outline of this study: (a) preparation of PhTAD-modified PIs by TAD-based click chemistry, followed by the formation of TAD–ZDMA cross-linkages *via* a radical mechanism. (b) Schematic illustration of the adhesion process *via* rearrangement of the ionic interaction among ZDMA.

detail using model experiments. Finally, the physical properties of the resulting cross-linked composites, including their dynamic viscoelasticity, tensile behaviour and adhesive strength, were examined. The obtained results demonstrate that the ZDMA cross-linking network *via* TAD units in PI is successfully formed *via* a radical mechanism, and that the resulting PI composites show unique physical properties, including improved adhesion strength.

Experimental

Materials

cis-1,4-Polyisoprene (PI; 98% c*is*-1,4 content; grade: IR2200) was purchased from ENEOS Materials Corp. Zinc dimethacrylate (ZDMA, Dymalink® 708) was obtained from Cray Valley Co., Ltd. Dichloroacetic acid, 4-phenyl-1,2,4-triazoline-3,5-dione (PhTAD), ethylene glycol dimethacrylate (EGDMA), zinc chloride ($ZnCl_2$), and zinc acetate ($Zn(OAc)_2$) were purchased from Tokyo Chemical Industry Co., Ltd. Dicumyl peroxide (DCP) was purchased from Sigma Aldrich Co. LLC. Tetrahydrofuran (THF), toluene, dichloromethane (CH_2Cl_2), methanol and *n*-heptane were purchased from Kanto Chemical Co., Ltd. 1,1,2,2-Tetrachloroethane-d_2 was purchased from Fujifilm Wako Pure Chemical Corp. *N*-(1,3-Dimethylbutyl)-*N*′-phenyl-*p*-phenylenediamine (6PPD, Nocrac 6C) was purchased from Ouchi Shinko Chemical Industrial Co., LTD.

Measurements

Gel-permeation-chromatography (GPC) measurements were carried out at 40 °C using a TOSOH HLC-8320 GPC system equipped with a guard column (TOSOH TSK guard column HXL-H), two separation columns (TOSOH TSK gel GMHXL), a differential refractive-index (RI) detector, and a UV detector. Tetrahydrofuran (THF) was used as the eluent at a flow rate of 0.6 mL min^{-1}. Polystyrene (PS) standards (M_w = 8 420 000 – 1010 g mol^{-1}) were used to calibrate the GPC system. Multi-angle light-scattering (MALS) measurements were conducted at 30 °C using a Wyatt DAWN as a MALS detector with a Wyatt Optilab as a RI detector. THF was used as the eluent at a flow rate of 1.0 mL min^{-1}. Differential-scanning-calorimetry (DSC) measurements were conducted using a DSC2500 (TA Instruments Inc.) instrument under an atmosphere of nitrogen at a heating rate of 20 °C min^{-1}. Fourier-transform infrared (FT-IR) spectra were recorded at room temperature using a Nicolet iS5 FT-IR spectrometer with a germanium-crystal-attenuated total-reflectance (ATR) attachment (Thermo Scientific Inc.). ^{1}H NMR spectra were measured in 1,1,2,2-tetrachloroethane-d_2 ($C_2D_2Cl_4$) at 300 K using a Bruker AVANCE III HD 600 MHz spectrometer. Rotorless-rheometer measurements were carried out at 145 °C using an RLR-4 (Toyo Seiki Manufacturing Co. Ltd) instrument under a pressure of 10 MPa with a fixed amplitude angle of ±1° and a frequency of 100 cpm. Dynamic-mechanical-analysis (DMA) tests were conducted on a GABO EPLEXOR (Netzsch) apparatus equipped with a 500 N load cell, using standard JIS-K6251 strip-shaped specimens (length: 40.0 mm; width: 4.7 mm). Temperature-sweep DMA tests were carried out in tensile mode with a fixed frequency of 15 Hz, a static strain of 6%, a dynamic strain of 0.4%, and a heating rate of 2 °C min^{-1} from −75 to 150 °C. The strain-sweep tests were conducted at 25 °C in tensile mode with a fixed frequency of 15 Hz, a static strain of 10%, and a dynamic strain range from 0.1 to 10%. Tensile tests were carried out at room temperature using an Instron 5965 (Instron) instrument equipped with a 5 kN load cell at a crosshead speed of 100 mm min^{-1}, using dumbbell-shaped ISO 37-4 specimens. Three measurements were performed for each sample. The fracture energy, W, was calculated using the equation $W = \int_0^{\varepsilon} \sigma(\varepsilon) d\varepsilon$. T-Peel adhesion tests were conducted at room temperature on an Instron 5965 (Instron) instrument equipped with a 5 kN load cell at a crosshead speed of 300 mm min^{-1} using laminated stripes (length: 75 mm; width: 10 mm). Two measurements were performed for each sample.

Preparation of TAD-modified PI samples

PI was dissolved in CH_2Cl_2 (0.033 g mL^{-1}), before a CH_2Cl_2 solution of PhTAD (0.02 g mL^{-1}) was added dropwise, and stirring was continued for 5 min at room temperature. The solution was then concentrated under reduced pressure until the volume was reduced to approximately one third of the original volume. The thus obtained solution was poured into methanol to precipitate the modified PI, which was then washed with methanol. Finally, the modified PI was dried under vacuum at 65 °C for 12 h. The resulting modified PIs are denoted as TAD-PI-1, TAD-PI-2, TAD-PI-3 and TAD-PI-4, which correspond to PhTAD loadings of 1.0, 2.0, 3.5 and 5.0 mol% relative to the isoprene monomer unit in the PI, respectively.

Mixing and curing conditions for the uncured rubber samples with ZDMA

PI or TAD-PIs (20 g, 100 phr) were mixed with different amounts of ZDMA for 10 min on a two-roll open mill with a roller speed of 15 rpm at 65 °C. The PI/ZDMA mixtures were further mixed with varying amounts of DCP for 2 min on the two-roll open mill with a roller speed of 15 rpm at 65 °C. The resulting samples were hot-pressed (145 °C, 15 MPa, 30 min) to give sheets with a thickness of ∼1 mm.

Mixing conditions for TAD-PI-4 with 6PPD and ZDMA

TAD-PI-4 (5.0 g, 100 phr) was mixed with 6PPD (0.25 g, 5 phr) for 3 min on a two-roll open mill with a roller speed of 15 rpm at 65 °C. Subsequently, the TAD-PI-4/6PPD mixture was further mixed with ZDMA (2.0 g, 40 phr) for 10 min on the two-roll open mill with a roller speed of 15 rpm at 65 °C.

Mixing conditions for TAD-PI-4 with $Zn(OAc)_2$

TAD-PI-4 (5.0 g, 100 phr) was mixed with $Zn(OAc)_2$ (2.0 g, 40 phr) for 10 min on a two-roll open mill with a roller speed of 15 rpm at 65 °C.

Mixing conditions for TAD-PI-4 with $ZnCl_2$ or EGDMA

A round-bottom flask was charged with TAD-PI-4 (5.0 g, 100 phr) and CH_2Cl_2 (100 mL). After TAD-PI-4 had dissolved completely, zinc chloride (2.0 g, 40 phr) or EGDMA (2.0 g, 40 phr) was added to the solution, which was subsequently stirred at room temperature for 30 min. The solutions were then cast onto mould-release films and placed under reduced pressure at room temperature for 12 h, followed by drying under vacuum at 50 °C for 2 h.

Dissolution study of cross-linked samples

The cross-linked sheets were cut into disc-shaped specimens with a diameter of 8.0 mm. The cut samples were immersed in 10 mL of toluene/dichloroacetic acid (v/v = 95/5)[43] and kept at room temperature for 4 days.

Preparation of T-peel test samples[43]

Two sheets of each of the prepared cross-linked rubber samples were attached to each other without any pretreatment or adhesive. To ensure a sufficient gripping area on the specimens for the T-peel tests, a thin piece of a poly(tetrafluoroethylene) (PTFE) film (length: 15–20 mm) was placed between the two sheets at the edge of the specimens. Then, the laminates were hot-pressed (145 °C, 15 MPa, 30 min) to give specimens of approximately 2 mm.

Results and discussion

Synthesis of TAD-PIs

To prepare TAD-PIs, PhTAD and PI were reacted in CH_2Cl_2 (Scheme 1).[85] After the red solution of PhTAD was added to the PI solution, it immediately became pale yellow, indicating that the reaction proceeded rapidly. The unmodified PI and the prepared TAD-PIs were characterized using ^{1}H NMR and FT-IR spectroscopy, as well as GPC and DSC measurements; the results are summarized in Table 1. The ^{1}H NMR spectra of the obtained TAD-PIs (Fig. 2 and Fig. S1† as well as Table S1†) showed the disappearance of the initial signals for PhTAD and the appearance of distinct new signals corresponding to the phenyl protons in the aromatic region as well as the methine proton at δ 2.77 ppm. The bound TAD content was calculated based on the integration ratio of the signal of the phenyl group protons at 7.63–7.30 ppm relative to that of the original olefinic proton of the *cis*-1,4 unit at 5.14 ppm (*cf.* eqn (S1)–(S3)†). The modification efficiency values were found to be 83.3, 85.5, 88.8 and 86.5% for TAD-PI-1, 2, 3, and 4, respectively. The M_n and M_w/M_n values of the PI and TAD-PI samples were determined using GPC. The M_n values of the TAD-PI samples decreased with increasing degree of TAD modification. The decrease in the apparent M_n upon TAD modification was attributed to the reduced hydrodynamic volume due to the interaction of intramolecular N–H···N hydrogen bonds originating from the TAD-derived urazole groups.[83,84] However, the MALS measurements confirmed a decrease in the M_n values with TAD modification (Table S2†), indicating that a main-chain scission occurred during the reaction of PI and TAD, presumably due to the generation of radical species from the TAD-derived urazole units.[85–87] The DSC measurements revealed that the glass-transition temperature (T_g) of the unmodified PI, TAD-PI-1, 2, 3 and 4 were −64.6, −63.3, −62.6, −61.7 and −61.2 °C, respectively (Fig. 3a). The increase in T_g with increasing degree of TAD modification was attributed to a decrease in the polymer-chain mobility induced by hydrogen bonding between the TAD-derived urazole groups.[82–85] The TAD modification of PI was also examined using IR spec-

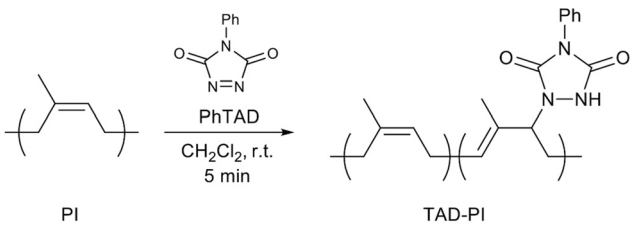

Scheme 1 Synthesis of TAD-PI.

Table 1 Characterization of PI and TAD-PIs

Polymer	Bound TAD [a] (mol%)	M_n [b]	M_w/M_n [b]	T_g [c] (°C)
PI	0	496 000	2.78	−64.6
TAD-PI-1	0.83	365 000	2.88	−63.3
TAD-PI-2	1.7	266 000	3.35	−62.6
TAD-PI-3	3.1	122 000	4.80	−61.7
TAD-PI-4	4.3	80 100	4.85	−61.2

[a] Determined by ^{1}H NMR spectroscopy. [b] Determined by GPC based on polystyrene standards (eluent: THF). [c] Determined by DSC.

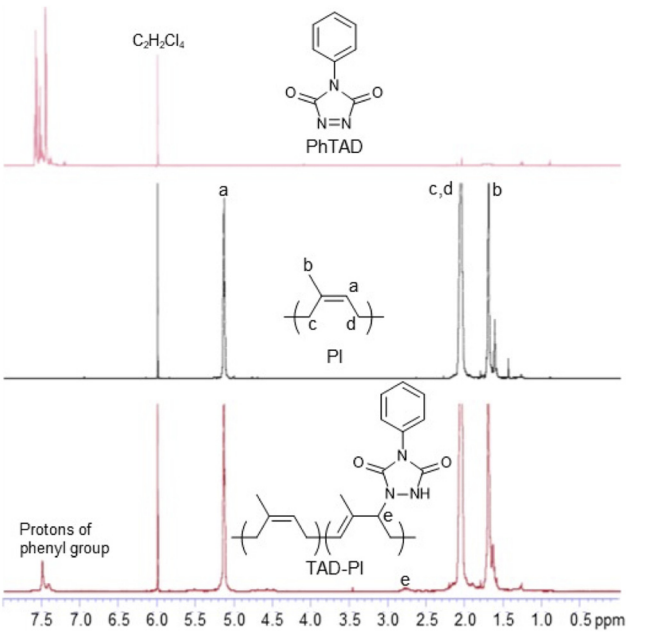

Fig. 2 ^{1}H NMR spectra of PhTAD, PI and TAD-PI-4 ($C_2D_2Cl_4$, 600 MHz).

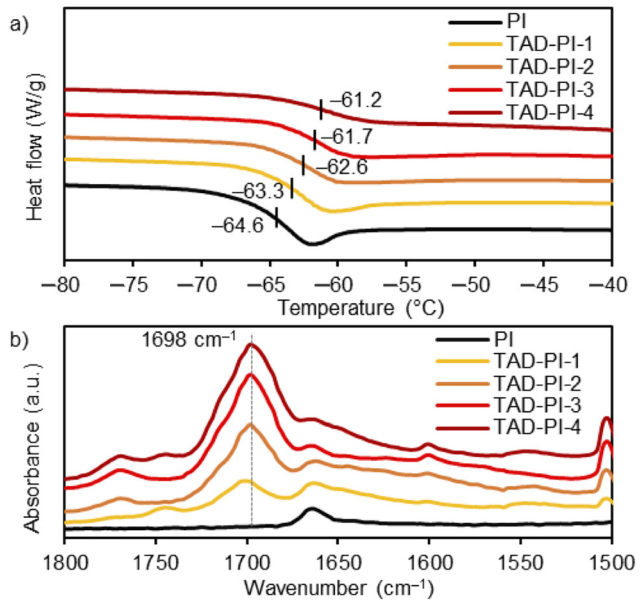

Fig. 3 Characterization of PI (black), TAD-PI-1 (yellow), TAD-PI-2 (orange), TAD-PI-3 (red) and TAD-PI-4 (dark red): (a) DSC curves and (b) ATR FT-IR spectra.

troscopy, in which the typical absorbance of the C=O stretching vibrations is observed around 1698 cm^{-1},[84,85] and the intensity of this peak increases with increasing degree of TAD modification (Fig. 3b).

Cross-linking of rubber samples

Cross-linked rubber composites were prepared using the unmodified PI and TAD-PIs; the formulations of all samples are summarized in Table 2. To prepare unmodified PI composites with varying degrees of cross-linking as control samples, 40 phr of ZDMA was mixed with 0.2, 0.6, 1.0 and 1.5 phr of dicumyl peroxide (DCP) (runs 1–4). The samples based on the TAD-PIs were prepared using 40 phr of ZDMA with TAD-PI-1, 2, 3 and 4, respectively (runs 5–8) to clarify the effect of the amount of bound TAD in the PI on the resulting physical properties. Additional samples were synthesized using 30 phr and 50 phr of ZDMA to gain insight into the impact of the amount of ZDMA incorporated on the mechanical properties (runs 9 and 10). The hot-pressing conditions were adjusted to provide a comparable level of cross-linking density between PI/Z40/DCP1.0 and TAD-PI-3/Z40, as evaluated by swelling experiments in *n*-heptane (Fig. S2†). To characterize the cross-linking of TAD–ZDMA, the elastic torque of the samples was analysed using a rheometer at 145 °C. The unmodified PI control composites prepared using the DCP-and-ZDMA-based curing system demonstrated an increase in elastic torque associated with cross-linking, whereby larger torque increases were observed for higher feed rates of DCP (Fig. 4a).[91] Increased elastic torque was also observed for the TAD-PI samples loaded with 40 phr of ZDMA (Fig. 4b), indicating the formation of a cross-linking network. Increasing amounts of bound TAD in the PI samples resulted in larger elastic torque, suggesting a higher degree of TAD–ZDMA cross-linking. The enhanced TAD–ZDMA cross-linking density was further confirmed through a swelling experiment with *n*-heptane, which revealed that the degree of swelling of the composites from TAD-PI-1–4 was consistent with the trend in their torque values (Fig. S3†). The effects of different ZDMA loadings on the elastic torque were also investigated using TAD-PI-4 (Fig. 4c). Relative to TAD-PI-4/Z40, TAD-PI-4/Z30 showed a lower elastic torque, while TAD-PI-4/Z50 exhibited a higher torque. These results suggest that the degree of TAD–ZDMA cross-linking is enhanced with increasing ZDMA loading.

Mechanistic study of the cross-linking of TAD–ZDMA

To clarify the cross-linking mechanism of the TAD-PI and ZDMA composites, several control composites were used with TAD-PI-4; the formulations of the samples are summarized in Table 3. To investigate the possibility of cross-linking *via* ionic or coordination bonding between the bound TAD units and the zinc ion in ZDMA, $ZnCl_2$ and $Zn(OAc)_2$ were used as alternative zinc sources for runs 11 and 12, respectively. TAD-PI-4/$Zn(OAc)_2$ was mixed using the open roll, but TAD-PI-4/$ZnCl_2$ was prepared by casting a CH_2Cl_2 solution of a TAD-PI-4/$ZnCl_2$ mixture due to the hygroscopic and metal-corrosive nature of $ZnCl_2$. The torque measurements using a rheometer at 145 °C revealed no increase in elastic torque for either sample (Fig. 4d and e), demonstrating that the TAD–ZDMA cross-linking is not due to ionic or coordination

Table 2 Formulation of the prepared cross-linked samples[a]

Run	1	2	3	4	5	6	7	8	9	10
Sample code	PI/Z40/DCP0.2	PI/Z40/DCP0.6	PI/Z40/DCP1.0	PI/Z40/DCP1.5	TAD-PI-1/Z40	TAD-PI-2/Z40	TAD-PI-3/Z40	TAD-PI-4/Z40	TAD-PI-4/Z30	TAD-PI-4/Z50
PI	100	100	100	100						
TAD-PI-1					100					
TAD-PI-2						100				
TAD-PI-3							100			
TAD-PI-4								100	100	100
DCP	0.2	0.6	1.0	1.5						
ZDMA	40	40	40	40	40	40	40	40	30	50

[a] The unit of the values (phr) refers to the weight fraction of the specified rubber component per 100 units of the base rubber.

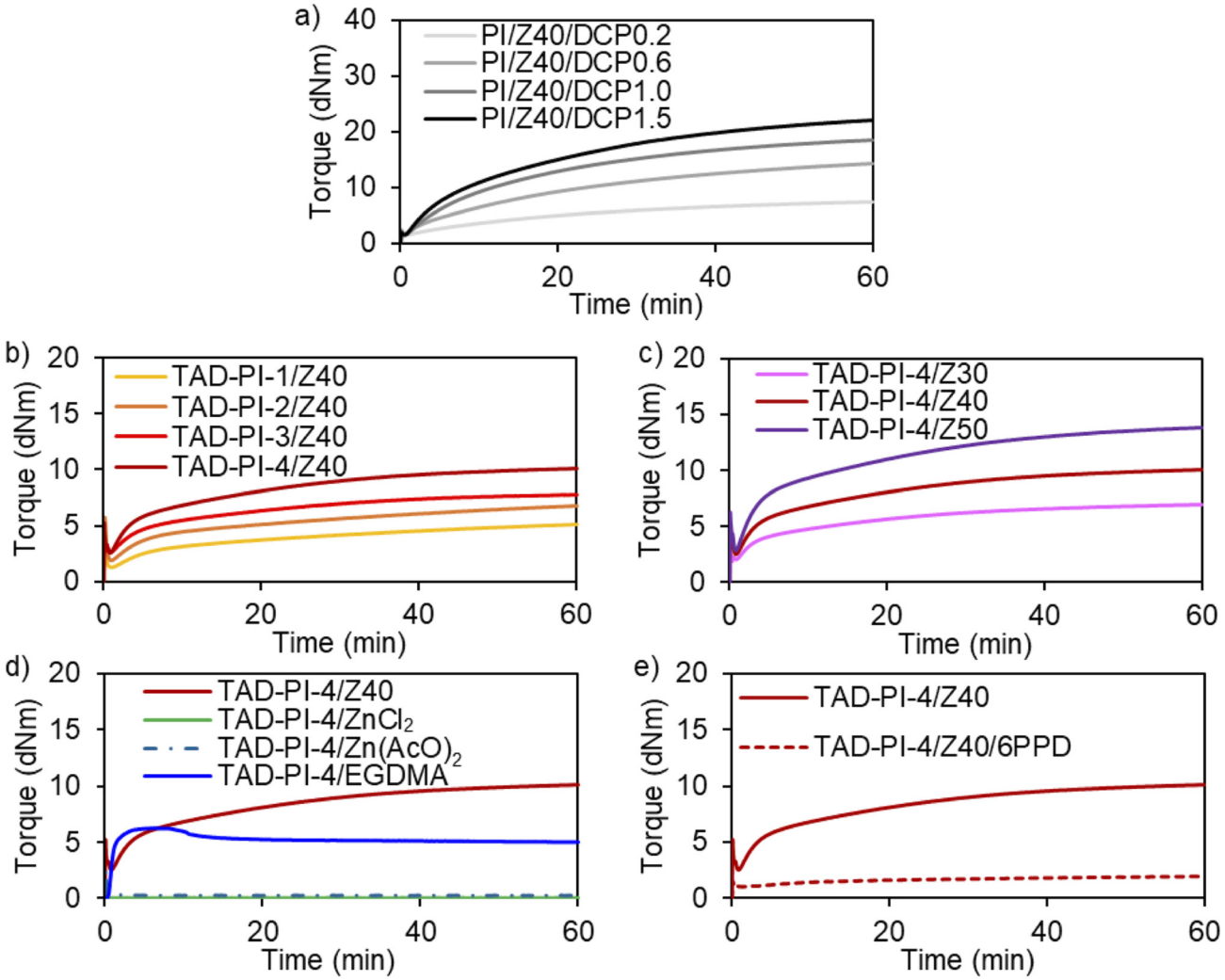

Fig. 4 Elastic-torque curves of rubber composites measured using a moving die rheometer at 145 °C: (a) control samples (PI/Z40/DCP), (b) effect of the amount of bound TAD in the PIs, (c) effect of the ZDMA content, (d) results for TAD-PI-4 with various types of chemicals and (e) the effect of the radical-trapping agent 6PPD.

Table 3 Formulation of the samples used for examining the cross-linking formation[a]

Run	11	12	13	14
Sample code	TAD-PI-4/$ZnCl_2$	TAD-PI-4/Zn$(OAc)_2$	TAD-PI-4/EGDMA	TAD-PI-4/Z40/6PPD
TAD-PI-4	100	100	100	100
ZDMA				40
$ZnCl_2$	40			
$Zn(OAc)_2$		40		
EGDMA			40	
6PPD				5

[a] The unit (phr) refers to the weight fraction of the specified rubber component per 100 units of the base rubber.

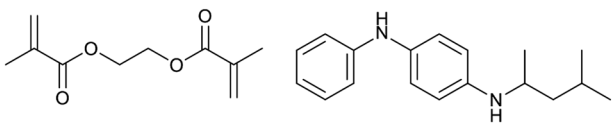

Fig. 5 Chemical structures of EGDMA (left) and 6PPD (right).

bonding between the TAD unit and the zinc atom. To investigate the possibility of cross-linking *via* a radical mechanism, a composite with 40 phr of EGDMA (Fig. 5; left) as a radically reactive bifunctional methacrylate was prepared (run 13) by casting a CH_2Cl_2 solution to avoid slippage of the sample on the open roll due to the large amount of liquid EGDMA. TAD-PI-4/EGDMA without a zinc source showed a rapid and significant increase in its elastic torque (Fig. 4d; blue line), suggesting that the cross-linking was formed *via* a radical mechanism. The mechanism was further verified by adding 5 phr of 6PPD (Fig. 5; right), a radical-trapping agent, to the TAD-PI-4/Z40 system (run 14); this composite was prepared using the open-mill method. The elastic torque for TAD-PI-4/

Z40/6PPD decreased drastically in comparison with that of TAD-PI-4/Z40 (Fig. 4e), further supporting the radical mechanism. Based on these results, a series of plausible reactions between the TAD-PIs and ZDMA is presented in Scheme 2. In the first step of cross-linking, the TAD-derived urazole units generate nitrogen radicals through transformation from rubber macroradicals or under thermal oxidation at elevated temperature,[85] followed by radical addition to the methacrylate units in ZDMA. The radical on ZDMA presumably further reacts with other ZDMA molecules, eventually producing grafted poly-ZDMA.[88,89,91] During this series of radical reactions, the cross-linkages would be formed through the reaction of the methacrylate units on both sides of ZDMA. This proposed radical mechanism is also supported by previous studies that demonstrate the generation of radicals in urazole moieties.[85–87]

To further examine the formation of TAD–ZDMA cross-linkages, dissolution tests were conducted for all the composites using a toluene/dichloroacetic acid mixture (*v*/*v* = 95/5) (Fig. 6).[43] Disc-shaped specimens with a diameter of 8.0 mm (Fig. 6a) were immersed in the solvent (Fig. 6b) and kept at room temperature for 4 days. All TAD-PI composites completely dissolved, and the solutions turned pale yellow (Fig. 6c), indicating that the TAD–ZDMA cross-links were dissociated by the acid. Notably, the control PI composites cured using DCP did not show dissolution behaviour, but instead exhibited swelling (Fig. 6c). These results demonstrate that the control composites contain direct C–C covalent cross-links among the PI main chains, while the TAD-PI/ZDMA composites mainly consist of dissociative TAD–ZDMA cross-linking. To further investigate the cross-linking mechanism, the dissolved fraction of TAD-PI-4/Z40 was analysed using ^{1}H NMR spectroscopy. The two sharp signals at 1.69 ppm and 1.47 ppm as well as the broad signals at 2.2–0.7 ppm corresponding to the methyl groups and methylene/methine groups in the reacted methacrylic groups, respectively, demonstrated that the composites consisted of a complex mixture, presumably including grafted poly-ZDMA (Fig. S4†).

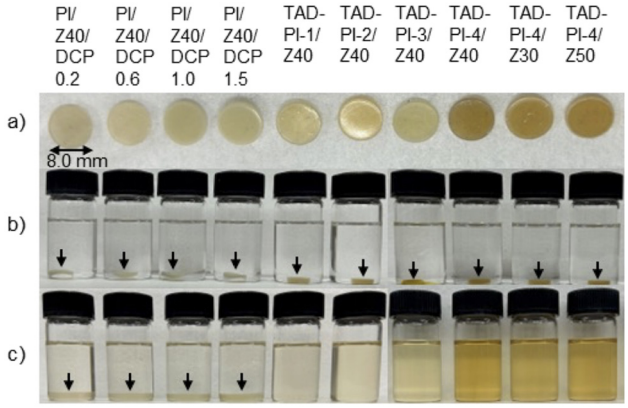

Fig. 6 Photographs documenting the dissolution and swelling behaviour of the cured rubber composites in toluene/dichloroacetic acid (*v*/*v* = 95/5): (a) prepared specimens, (b) beginning of the test and (c) after soaking at room temperature for 4 days.

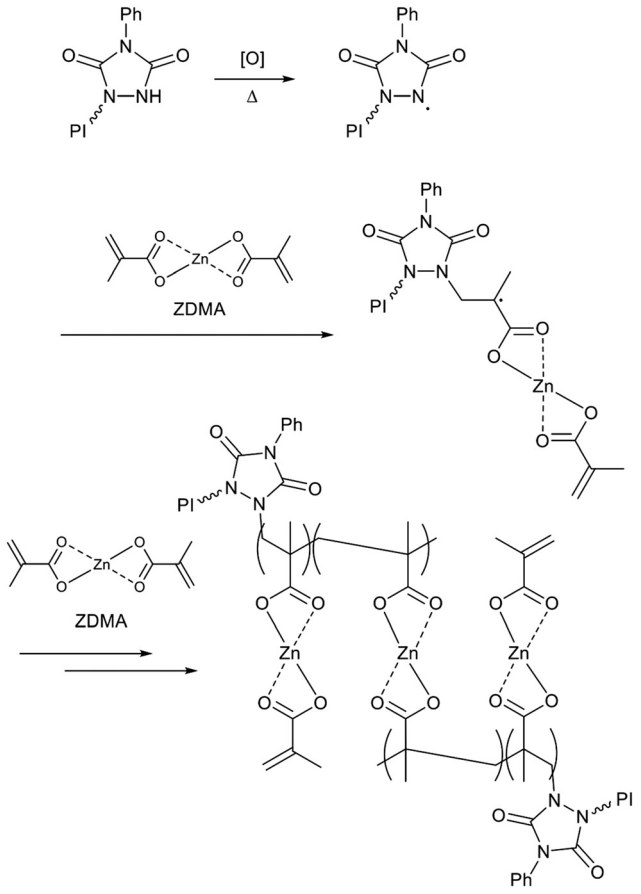

Scheme 2 Plausible mechanism for the formation of cross-links between TAD-PIs and ZDMA.

DMA measurements

To investigate the temperature dependence of the prepared samples, temperature-sweep DMA tests were carried out from −75 to 150 °C (Fig. 7). The measurements for the control PI composites showed that increased DCP loading leads to an increase in the E' values of the rubbery plateau region (Fig. 7a) and a decrease in the tan δ values (Fig. 7b); these changes are due to the increased degree of cross-linking. Additionally, the measurements of the TAD-PIs revealed that increasing bound TAD content afforded a significant increase in the E' values in the rubbery plateau region (Fig. 7c), indicating an increase in the degree of cross-linking. In addition, the tan δ curve shifts toward higher temperatures with increasing bound TAD content (Fig. 7d), in agreement with the trend in the T_g values measured using DSC. Furthermore, the remarkable decrease in the tan δ peak values and broadening of the peak shapes observed with increasing bound TAD content suggest that ZDMA acts as a reinforcing filler and forms a bound rubber layer[43,96] *via* the formation of TAD–ZDMA bonds. Notably, the E' values of the TAD-PI composites gradually decrease even in

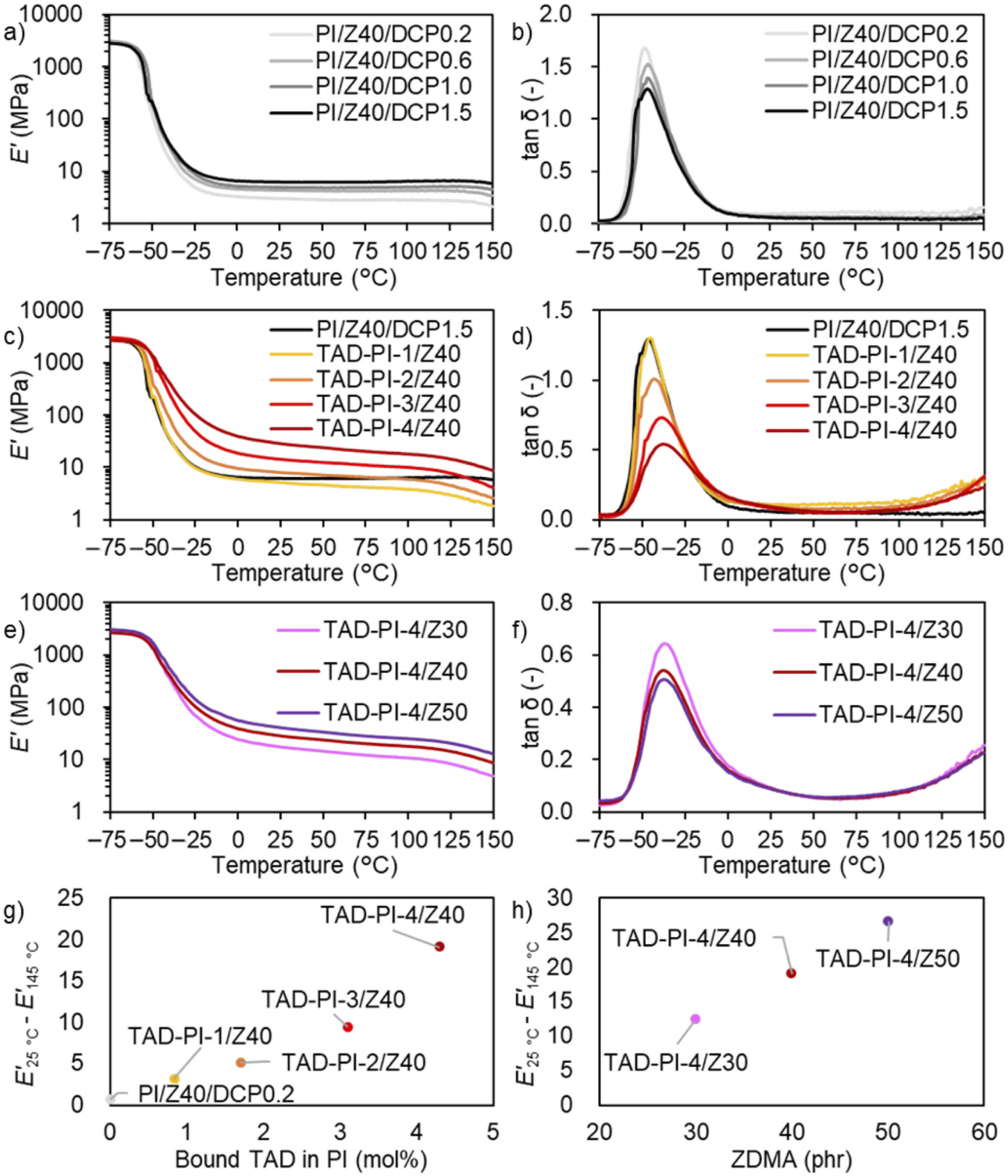

Fig. 7 Temperature dependence of the viscoelasticity: (a) E' of control samples (PI/Z40/DCP), (b) tan δ of control samples (PI/Z40/DCP), (c) effect of the amount of bound TAD in the PI on E', (d) effect of the amount of bound TAD in the PI on tan δ, (e) effect of the loaded ZDMA content on E', (f) effect of the loaded ZDMA content on tan δ, (g) effect of the amount of bound TAD in the PI on the difference between E' at 25 °C and E' at 145 °C and (h) effect of the ZDMA content on the difference between E' at 25 °C and E' at 145 °C.

the rubbery plateau region, and this decrease becomes more intense above 110 °C. The gradual decrease in the E' values in the rubbery plateau region presumably reflects the dissociation of relatively weak cross-linking such as the ionic interaction among zinc ions and hydrogen bonds[82–85] between TAD-derived urazole moieties. Furthermore, the rapid decrease

of E' above 110 °C may be the effect of ligand exchange among ZDMA, because the control PI/ZDMA/DCP composites also show a similar decrease at temperatures above the rubbery plateau region. The impact of the ZDMA loading content on E' and tan δ was also investigated using TAD-PI-4. The E' values in the rubbery plateau region increase with increasing ZDMA content (Fig. 7e), indicating an increase in the degree of cross-linking *via* TAD–ZDMA bonding. A gradual decrease in E' values in the rubbery plateau region is also observed even with increased ZDMA content. The intensity of the tan δ peak attributed to the glass transition decreases with increasing ZDMA content (Fig. 7f), indicating an increase of the formation of a bound rubber layer *via* TAD–ZDMA bonding. Based on the above discussion, the difference between the values of E' at high and low temperatures is expected to be a predictor of the degree of dissociation of the weak cross-linking.[43] The differences between the values of E' at 25 °C and 145 °C, denoted as $E'_{25°C} - E'_{145°C}$, were plotted to investigate their relationship with the bound TAD content and the amount of ZDMA in the PIs (Fig. 7g and h). $E'_{25°C} - E'_{145°C}$ obviously increases both with increasing bound TAD content and ZDMA amount, demonstrating that the decrease in the E' values at elevated temperature reflects the dissociation of the cross-linking involving bound TAD units. In contrast, the $E'_{25°C} - E'_{145°C}$ values of the control PI composites are much lower than those of the TAD-PI composites even though both contain ZDMA. Unlike the TAD-PI composites, the control PI composites feature direct C–C covalent cross-linkages among the PI main chains, as demonstrated by the dissolution experiments (*vide supra*). The presence of the permanent cross-linkages presumably restricts polymer chain mobility, which preserves the ionic network even at high temperature.

To further investigate the impact of TAD–ZDMA cross-linking on the dynamic mechanical behaviour, strain-sweep DMA tests were conducted at strains ranging from 0.1% to 10% (Fig. 8). For the control PI composites, a slight increase in the E' values with increasing DCP loading is observed (Fig. 8a), in the same manner as in the temperature-sweep DMA measurements. Importantly, these control composites show almost no decrease in E' (Payne effect)[97] with increasing strain, indicating the absence of a significant network of ZDMA particles. On the other hand, TAD-PI composites TAD-PI-1 to TAD-PI-3 show a slight decrease in E' with increasing strain (Fig. 8b). Notably, TAD-PI-4/Z40 shows an obvious Payne effect, demonstrating that the rich content of bound TAD in the PIs enhanced the ZDMA–ZDMA filler interaction[43,92,93] *via* TAD–ZDMA bonding. The measurements for TAD-PI-4 with varying ZDMA contents revealed that the Payne effect is significantly amplified when the ZDMA content is increased (Fig. 8c) due to the formation of strong ZDMA–ZDMA filler interactions.[91] Based on these results, it is obvious that ZDMA plays important roles as both a cross-linking agent and a reinforcing filler in the TAD–ZDMA cross-linking system.

Tensile tests

To investigate the impact of the TAD–ZDMA linkages on the mechanical strength, tensile tests were conducted (Fig. 9); the mechanical properties are summarized in Table 4. Stress–strain curves for the control PI composites showed that the elastic modulus values increased with the amount of DCP (Fig. 9a); the same tendency was observed in the conventional DCP–ZDMA curing system.[91] As shown in Fig. 9b, the moduli of the TAD-PI composites clearly increase with increasing amount of bound TAD due to increased cross-linking, with 100% modulus values of 1.61, 2.67, 4.60 and 6.17 MPa for composites TAD-PI-1, 2, 3 and 4, respectively. The trend in the moduli of the TAD-PI samples is consistent with their swelling degrees in *n*-heptane (Fig S5†). Additionally, fracture-energy values of 28.8, 42.1, 47.3 and 37.6 MJ m^{-3} were measured for composites TAD-PI-1, 2, 3 and 4, respectively. These results suggest that a bound TAD content of approximately 3.1 mol% (*i.e.*, TAD-PI-3) is optimum in terms of the fracture energy.

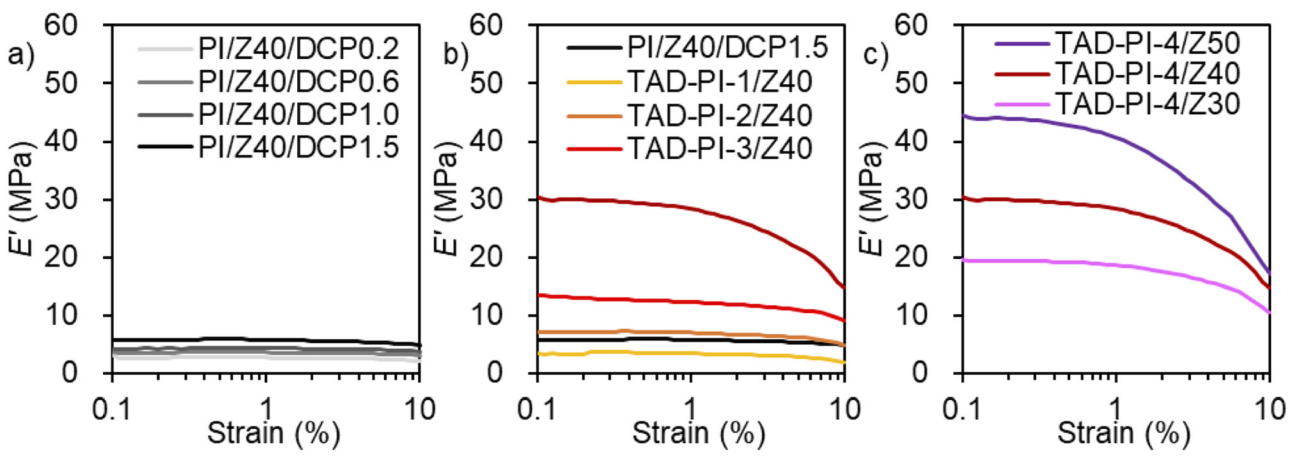

Fig. 8 Strain dependence of E': (a) control samples (PI/Z40/DCP), (b) effect of the amount of bound TAD in the PI on E' and (c) effect of the loaded ZDMA content on E'.

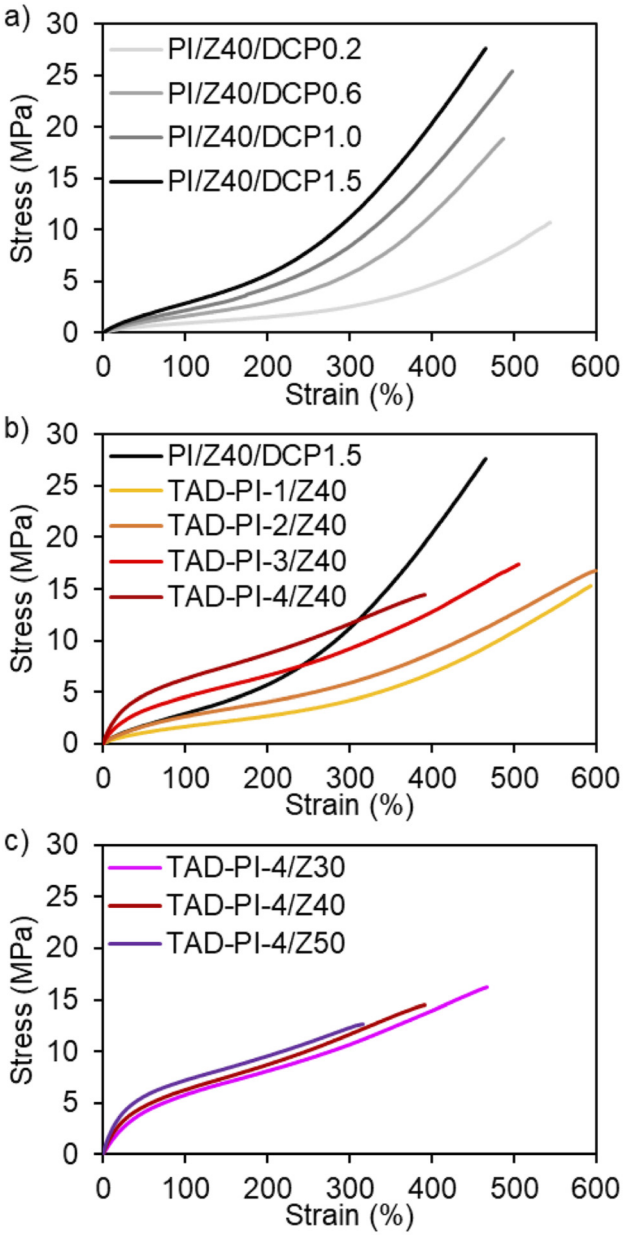

Fig. 9 Stress–strain curves: (a) control samples (PI/Z40/DCP), (b) effect of the amount of bound TAD in the PIs and (c) the effect of loaded ZDMA content.

Importantly, the fracture-energy value of TAD-PI-3/Z40 (Table 1, run 7) reached the same level as that of the PI/ZDMA/DCP system (run 3). The TAD-PI samples also tended to show higher 100%-modulus values than the control PI composites with comparable swelling rates in *n*-heptane (Fig. S5†). For example, the swelling degrees of PI/Z40/DCP0.2, PI/Z40/DCP0.6 and PI/Z40/DCP1.5 are comparable to those of TAD-PI-1/Z40, TAD-PI-2/Z40 and TAD-PI-3/Z40, respectively, albeit their 100%-modulus values are notably lower. This indicates that the swelling rate of the TAD-PI/Z40 samples underestimates the actual cross-linking density. These results suggest the presence of cross-linkages consisting of weak bonds, *e.g.*, hydrogen bonds[82–85] and electrostatic interactions among the TAD units and ZDMA, which dissociate during swelling with *n*-heptane. Moreover, the TAD-PI samples (except for TAD-PI-1/Z40) tend to show lower values of tensile strength at break (T_b) relative to the PI control samples with a similar swelling degree in *n*-heptane (Fig. S6†). For example, the T_b values of PI/Z40/DCP1.0 and TAD-PI-3/Z40 are 26.3 and 18.2 MPa, respectively, even though these samples showed comparable swelling rates. The relatively lower T_b values for the composites of TAD-PI-2, 3, and 4 compared to those of the control PI samples are probably due to suppressed strain-induced crystallization (Fig. S7†), which is a unique characteristic of *cis*-1,4-polyisoprene,[98] due to the increased bound TAD amount. Fig. 9c summarizes the impact of the ZDMA loading on the stress–strain curve; fracture-energy values of 38.5, 37.6 and 25.0 MJ m^{-3} were found for TAD-PI-4 composites with 30 phr, 40 phr and 50 phr of ZDMA, respectively, indicating that a high loading of ZDMA gives brittle composites in this system.

Adhesion performance

The above discussion clearly reveals that the TAD–ZDMA cross-links dissociate with increasing temperature, and accordingly, suggest the thermal malleability of the TAD-PI composites with ZDMA. Thus, we examined the direct adhesion of TAD-PI composites using a hot-pressing process. For that purpose, two cross-linked sheets of each sample were stacked and remoulded at 145 °C under 15 MPa for 30 min, and then T-peel tests were conducted using the adhered samples (Fig. 10). The control PI samples PI/Z40/DCP0.6 and PI/Z40/DCP1.0 exhibited almost the same level of peeling force; these

Table 4 Moduli and fracture parameters of the cross-linked samples shown in Fig. 9; values in parentheses refer to the standard deviation

Run/sample code	100% modulus (MPa)	300% modulus (MPa)	Elongation at break (E_b) (%)	Tensile strength at break (T_b) (MPa)	Fracture energy (MJ m^{-3})
1/PI/Z40/DCP0.2	0.99 (0.04)	2.71 (0.17)	541 (13)	11.5 (0.58)	19.2 (0.94)
2/PI/Z40/DCP0.6	1.71 (0.02)	6.05 (0.28)	475 (18)	18.6 (1.16)	28.1 (2.52)
3/PI/Z40/DCP1.0	2.24 (0.07)	8.59 (0.39)	502 (6.8)	26.3 (1.92)	44.4 (3.74)
4/PI/Z40/DCP1.5	2.91 (0.01)	11.7 (0.47)	451 (16)	27.3 (1.95)	43.3 (4.21)
5/TAD-PI-1/Z40	1.61 (0.03)	4.24 (0.10)	580 (42)	15.2 (1.69)	28.8 (5.44)
6/TAD-PI-2/Z40	2.67 (0.03)	5.94 (0.08)	596 (20)	16.6 (0.83)	42.1 (3.41)
7/TAD-PI-3/Z40	4.60 (0.08)	9.35 (0.33)	525 (31)	18.2 (0.86)	47.3 (4.78)
8/TAD-PI-4/Z40	6.17 (0.10)	11.2 (0.30)	423 (24)	14.9 (0.44)	37.6 (2.87)
9/TAD-PI-4/Z30	5.81 (0.07)	11.0 (0.37)	434 (28)	15.8 (1.15)	38.5 (4.32)
10/TAD-PI-4/Z50	7.28 (0.11)	11.8 (0.38)	304 (23)	12.1 (0.46)	25.0 (2.21)

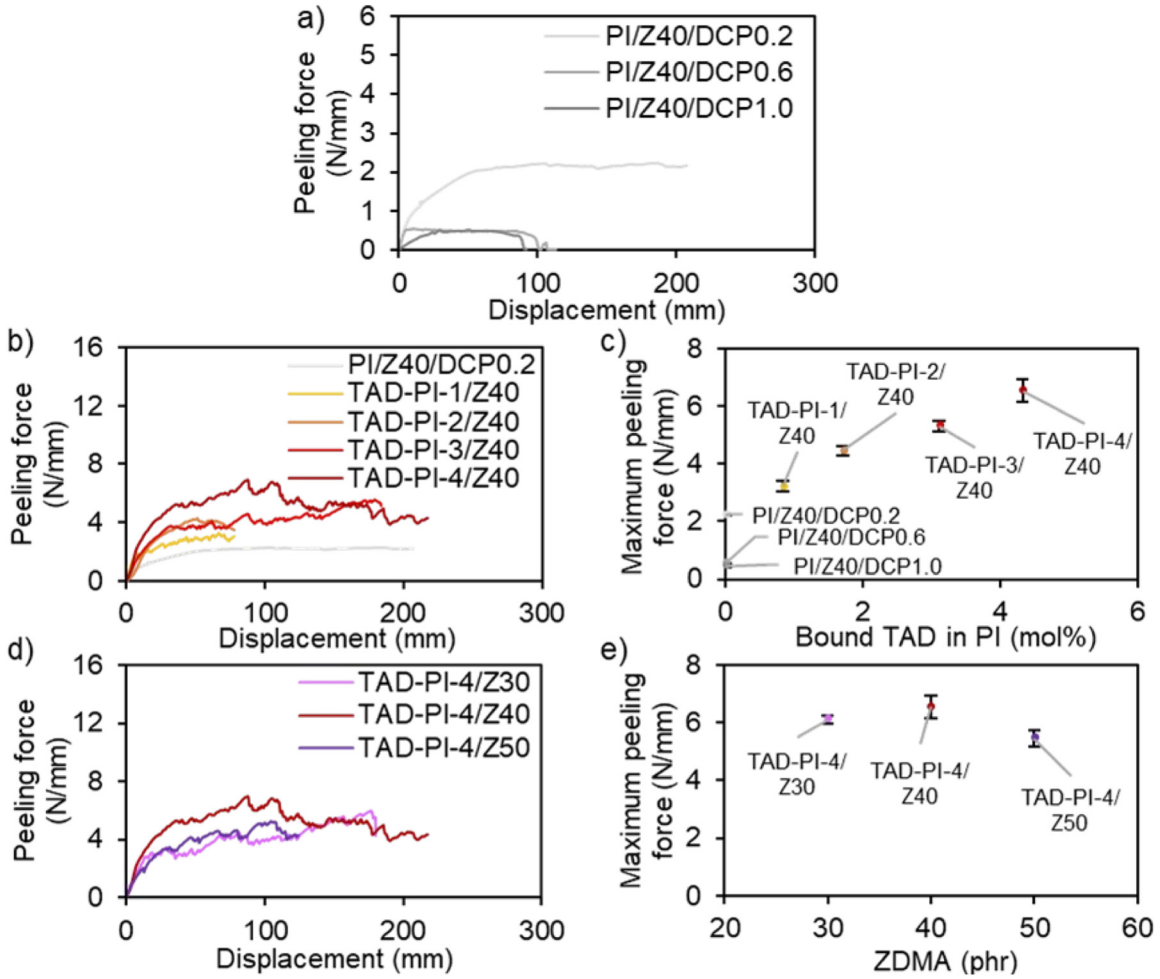

Fig. 10 T-peel test results: (a) control samples (PI/Z40/DCP), (b) effect of the amount of bound TAD in the PIs, (c) relationship between the maximum peeling force and the amount of bound TAD in the PIs, (d) effect of the loaded ZDMA content and (e) relationship between the maximum peeling force and the loaded ZDMA content.

values were lower than the peeling force of PI/Z40/DCP0.2 with a lower degree of cross-linking (Fig. 10a), indicating that a low cross-linking density is preferable for adhesion due to the mobility of the polymer chains. In contrast, the composites of TAD-PI with ZDMA clearly show higher peeling forces than the control samples cured with DCP, and the maximum peeling force dramatically increased with increasing amount of bound TAD in the PIs (Fig. 10b and c). The increase in peeling force with increasing amount of bound TAD can probably be rationalized in terms of the increase in the degree of TAD-ZDMA dissociative cross-linking. The impact of the ZDMA content on the peeling force was also investigated; the peeling force values are 6.11, 6.55 and 5.45 N mm^{-1} for the TAD-PI-4 composites prepared with 30, 40 and 50 phr of ZDMA, respectively. Both decreasing the ZDMA feed to 30 phr (TAD-PI-4/Z30) and increasing it to 50 phr (TAD-PI-4/Z50) resulted in a slight decrease in the maximum peeling-force value to 6.11 and 5.45, respectively (Fig. 10d and e), indicating that 40 phr of ZDMA is the optimum feed value for adhesion strength in this study. The relationships between the resulting maximum peeling force and the amount of bound TAD in the PI as well as the ZDMA content are summarized in Fig. 10c and e, respectively.

We have previously reported the good relationship between the maximum peeling force and $E'_{25°C} - E'_{145°C}$, which is a predictor of the degree of dissociative cross-links.[43] Based on the results of the adhesion tests, we examined whether the aforementioned correlation holds true for this system as well. A positive correlation was observed between the maximum peeling force and $E'_{25°C} - E'_{145°C}$ for most of the control PI/ZDMA/DCP composites and TAD-PI/ZDMA composites (Fig. 11). Only the point for TAD-PI-4/Z50 was an exception to the correlation. This is presumably explained by its high E' value at 145 °C, which was attributed to its too-high degree of ZDMA cross-linking to form poly-ZDMA. These results indicate that both the degree of dissociative crosslinking and the total degree of cross-linking at the adhesion temperature are significant for controlling the adhesion strength in the TAD–ZDMA cross-linking system.

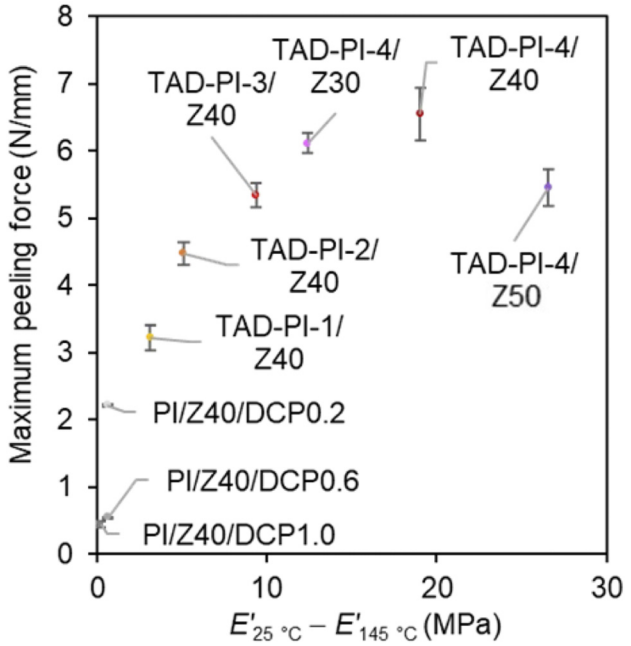

Fig. 11 Relationship between the maximum peeling force and the difference between E' at 25 °C and E' at 145 °C as a predictor of the degree of dissociation of the TAD–ZDMA cross-linking.

Conclusion

To achieve direct adhesion between cross-linked *cis*-1,4-polyisoprene (PI) rubbers without pretreatment of the rubber surfaces or the use of adhesives, we designed novel functionalized PI composites that contain ionic dissociative cross-linkages with zinc dimethacrylate (ZDMA). These composites were prepared *via* triazolinedione (TAD)-based click reactions using 4-phenyl-1,2,4-triazoline-3,5-dione (PhTAD), followed by the addition of ZDMA and a thermal curing process. The compounding study confirmed the formation of cross-linkages between the TAD units on the PIs and ZDMA through the elastic-torque curves of the rubber composites. Model experiments using zinc chloride ($ZnCl_2$), zinc acetate ($Zn(OAc)_2$), ethylene glycol dimethacrylate (EGDMA) and *N*-(1,3-dimethylbutyl)-*N*′-phenyl-*p*-phenylenediamine (6PPD) revealed that the cross-linking between TAD-PI and ZDMA proceeds *via* a radical mechanism. Furthermore, dissolution experiments with toluene/dichloroacetic acid demonstrated that the TAD-PI/ZDMA composites consist mainly of dissociative ionic cross-linkages.

The resulting TAD–ZDMA cross-linked PIs show a unique decrease in E' and increase in tan δ with increasing temperature in temperature-sweep DMA measurements, most likely due to dynamic dissociation of the ionic interactions *via* TAD–ZDMA linkages. The parameter $E'_{25°C} - E'_{145°C}$ was shown to serve as a predictor of the degree of dissociation of the TAD–ZDMA linkages. Strain-sweep DMA measurements showed a typical Payne effect for the TAD-PI/ZDMA composites, demonstrating that ZDMA plays the role of both a cross-linking agent and reinforcing filler. Tensile tests revealed that the elastic moduli of the TAD-PI/ZDMA composites are enhanced with increasing degree of TAD modification, and that their fracture energy is comparable to that of the conventional peroxide-cured sample. Finally, direct adhesion between the cross-linked rubbers was demonstrated, and the TAD–ZDMA cross-linked samples showed improved adhesion strength attributed to the dissociation of weak ionic cross-linking.

We have successfully established a novel system for direct adhesion between cross-linked polyisoprene rubbers. We are convinced that this study will not only accelerate the development of new rubber bonding technologies, but also contribute to the improvement of rubber repair processes, which could help achieve a circular economy with the reduction of rubber waste.

Author contributions

K.K., Y.K., K.T., A.T. and H.O. conceived the concept and designed the experiments. K.K. performed the experiments and analysed the data. Y.K. conducted the X-ray measurements and analysed the data. K.K., Y.K., K.T., A.T. and H.O. wrote the manuscript.

Data availability

The data supporting this article have been included as part of the ESI.†

Conflicts of interest

There are no conflicts to declare.

Acknowledgements

This work was supported by JST-Mirai Program Grant Number JPMJMI18A2, Japan. We extend our gratitude to Dr Hiromasa Yamashita for his valuable assistance and insights into crystallization analysis.

References

1 D. K. Kotnee and A. K. Bhowmick, *Rubber to Rubber Adhesion*, Scrivener Publishing LLC, Beverly, 2021.
2 R.-J. Chang and A. N. Gent, *J. Polym. Sci., Polym. Phys. Ed.*, 1981, **19**, 1619–1633.
3 A. K. Bhowmick and A. N. Gent, *Rubber Chem. Technol.*, 1984, **57**, 216–226.
4 H. Chun and A. N. Gent, *J. Polym. Sci., Part B: Polym. Phys.*, 1996, **34**, 2223–2229.
5 F. Ruch, M. O. David and M. F. Vallat, *J. Polym. Sci., Part B: Polym. Phys.*, 2000, **38**, 3189–3199.

6 S. Nakane, *Nippon Gomu Kyokaishi*, 2012, **85**, 204–207.
7 Indriasari, J. Noordermeer and W. Dierkes, *Appl. Sci.*, 2021, **11**, 9834.
8 G. Ferrer, *Resour., Conserv. Recycl.*, 1997, **19**, 221–255.
9 A. Shanbag and S. Manjare, *J. Sustain. Dev. Energy Water Environ. Syst.*, 2020, **8**, 22–34.
10 D. Dobrotă, G. Dobrotă and T. Dobrescu, *J. Cleaner Prod.*, 2020, **260**, 121141.
11 J. Gaidhane, I. Ullah and A. Khalatkar, *Mater. Today: Proc.*, 2022, **60**, 2257–2261.
12 V. Bijina, P. J. Jandas, S. Joseph, J. Gopu, K. Abhitha and H. John, *Polym. Bull.*, 2023, **80**, 8215–8244.
13 M. Hojo, S. Tahara and H. Kitano, *Nippon Gomu Kyokaishi*, 2024, **97**, 263–269.
14 S. Utrera-Barrios, R. Verdejo, M. A. López-Manchado and M. Hernández Santana, *Mater. Horiz.*, 2020, **7**, 2882–2902.
15 P. K. Behera, S. Mohanty and V. K. Gupta, *Polym. Chem.*, 2021, **12**, 1598–1621.
16 J. Xu, L. Zhu, Y. Nie, Y. Li, S. Wei, X. Chen, W. Zhao and S. Yan, *Materials*, 2022, **15**, 5993.
17 B. Li, P.-F. Cao, T. Saito and A. P. Sokolov, *Chem. Rev.*, 2023, **123**, 701–735.
18 M. Das, A. R. Parathodika, P. Maji and K. Naskar, *Eur. Polym. J.*, 2023, **186**, 111844.
19 S. Utrera-Barrios, R. Verdejo, M. A. López-Manchado and M. Hernández Santana, *Eur. Polym. J.*, 2023, **190**, 112023.
20 D. Y. S. Low, J. Supramaniam, W. D. Leong, A. Soottitantwat, T. Charinpanitkul, W. Tanthapanichakoon, S. Manickam, K. W. Tan, B. H. Goh and S. Y. Tang, *Mater. Today Sustain.*, 2023, **24**, 100545.
21 O. Olejnik and A. Masek, *J. Saudi Chem. Soc.*, 2023, **27**, 101676.
22 N. M. Kanafi, A. A. Ghani, N. A. Rahman, A. A. Aziz and S. M. Sapuan, *J. Mater. Sci.*, 2023, **58**, 608–635.
23 K. Chino and M. Ashiura, *Macromolecules*, 2001, **34**, 9201–9204.
24 C.-C. Peng and V. A. Abetz, *Macromolecules*, 2005, **38**, 5575–5580.
25 J. Liu, S. Wang, Z. Tang, J. Huang, B. Guo and G. Huang, *Macromolecules*, 2016, **49**, 8593–8604.
26 J. Huang, L. Zhang, Z. Tang, S. Wu, N. Ning, H. Sun and B. Guo, *Macromol. Rapid Commun.*, 2017, **38**, 1600678.
27 Y. Shoda, D. Aoki, K. Tsunoda and H. Otsuka, *Polymer*, 2020, **202**, 122700.
28 Z. Xie, B.-L. Hu, R.-W. Li and Q. Zhang, *ACS Omega*, 2021, **6**, 9319–9333.
29 Z. Tang, Y. Chen, C. Zhang, S. Wu, B. Guo and L. Zhang, *Polym. Int.*, 2023, **72**, 783–789.
30 L. Chen, J. Xu, M. Zhu, Z. Zeng, Y. Song, Y. Zhang, X. Zhang, Y. Deng, R. Xiong and C. Huang, *Mater. Horiz.*, 2023, **10**, 4000–4032.
31 T.-Y. Su, L.-W. Su, Z. Zhao, R.-G. Xing, X. Ge, G.-F. Pan and J.-X. Bao, *ACS Appl. Polym. Mater.*, 2024, **6**, 9763–9770.
32 C. Li, Y. Wang, Z. Yuan and L. Ye, *Appl. Surf. Sci.*, 2019, **484**, 616–627.
33 D. Mozhdehi, S. Ayala, O. R. Cromwell and Z. Guan, *J. Am. Chem. Soc.*, 2014, **136**, 16128–16131.
34 C.-H. Li, C. Wang, C. Keplinger, J.-L. Zuo, L. Jin, Y. Sun, P. Zheng, Y. Cao, F. Lissel, C. Linder, X.-Z. You and Z. Bao, *Nat. Chem.*, 2016, **8**, 618–624.
35 X. Zhang, Z. Tang, B. Guo and L. Zhang, *ACS Appl. Mater. Interfaces*, 2016, **8**, 32520–32527.
36 Y.-L. Rao, A. Chortos, R. Pfattner, F. Lissel, Y.-C. Chiu, V. Feig, J. Xu, T. Kurosawa, X. Gu, C. Wang, M. He, J. W. Chung and Z. Bao, *J. Am. Chem. Soc.*, 2016, **138**, 6020–6027.
37 Z. Tang, J. Huang, B. Guo, L. Zhang and F. Liu, *Macromolecules*, 2016, **49**, 1781–1789.
38 M. Das, S. Pal and K. Naskar, *eXPRESS Polym. Lett.*, 2020, **14**, 860–880.
39 M. Mareliati, L. Tadiello, S. Guerra, L. Giannini, S. Schrettl and C. Weder, *Macromolecules*, 2022, **55**, 5164–5175.
40 S. Mandal, F. Simon, S. S. Banerjee, L. B. Tunnicliffe, C. Nakason, C. Das, M. Das, K. Naskar, S. Wiessner, G. Heinrich and A. Das, *ACS Appl. Polym. Mater.*, 2021, **3**, 1190–1202.
41 Q. Wang, Y. Shi, Q. Li and C. Wu, *Eur. Polym. J.*, 2021, **150**, 110415.
42 Q. Wang, W. Wang, Q. Li and C. Wu, *Ind. Eng. Chem. Res.*, 2021, **60**, 2163–2177.
43 K. Kotani, K. Tsunoda and H. Otsuka, *RSC Appl. Polym.*, 2023, **1**, 229–242.
44 H. Park, T. Kang, H. Kim, J.-C. Kim, Z. Bao and J. Kang, *Nat. Commun.*, 2023, **14**, 5026.
45 L. Cao, Z. Gong, C. Liu, J. Fan and Y. Chen, *Comput. Sci. Technol.*, 2021, **207**, 108750.
46 A. Harada, Y. Takashima and M. Nakahata, *Acc. Chem. Res.*, 2014, **47**, 2128–2140.
47 G. Sinawang, M. Osaki, Y. Takashima, H. Yamaguchi and A. Harada, *Chem. Commun.*, 2020, **56**, 4381–4395.
48 Z. Lei, H. Chen, S. Huang, L. Wayment, Q. Xu and W. Zhang, *Chem. Rev.*, 2024, **124**, 7829–7906.
49 N. Van Herck and F. E. Du Prez, *Macromolecules*, 2018, **51**, 3405–3414.
50 P. Tanasi, M. Hernández Santana, J. Carretero-González, R. Verdejo and M. A. López-Manchado, *Polymer*, 2019, **175**, 15–24.
51 A. L. Dobson, N. J. Bongiardina and C. N. Bowman, *ACS Appl. Polym. Mater.*, 2020, **2**, 1053–1060.
52 B. T. Michal, E. J. Spencer and S. J. Rowan, *ACS Appl. Mater. Interfaces*, 2016, **8**, 11041–11049.
53 L. M. Polgar, M. van Duin, A. A. Broekhuis and F. Picchioni, *Macromolecules*, 2015, **48**, 7096–7105.
54 A. Takahashi, R. Goseki, K. Ito and H. Otsuka, *ACS Macro Lett.*, 2017, **6**, 1280–1284.
55 A. Tsuruoka, A. Takahashi, D. Aoki and H. Otsuka, *Angew. Chem., Int. Ed.*, 2020, **59**, 4294–4298.
56 S. Kataoka, A. Tsuruoka, D. Aoki and H. Otsuka, *ACS Appl. Polym. Mater.*, 2021, **3**, 888–895.

57 L. L. Robinson, E. S. Taddese, J. L. Self, C. M. Bates, J. Read de Alaniz, Z. Geng and C. J. Hawker, *Macromolecules*, 2022, **55**, 9780–9789.
58 M. Du, H. A. Houck, Q. Yin, Y. Xu, Y. Huang, Y. Lan, L. Yang, F. E. Du Prez and G. Chang, *Nat. Commun.*, 2022, **13**, 3231.
59 C.-C. Wang, M.-J. Xie, R. Zhang, J. Cao, M.-Z. Tang and Y.-X. Xu, *Polymer*, 2023, **273**, 125854.
60 I. Mora-Barrantes, M. A. Malmierca, J. L. Valentin, A. Rodriguez and L. Ibarra, *Soft Matter*, 2012, **8**, 5201–5213.
61 A. Das, A. Sallat, F. Böhme, M. Suckow, D. Basu, S. Wießner, K. W. Stöckelhuber, B. Voit and G. Heinrich, *ACS Appl. Mater. Interfaces*, 2015, **7**, 20623–20630.
62 C. Xu, L. Cao, X. Huang, Y. Chen, B. Lin and L. Fu, *ACS Appl. Mater. Interfaces*, 2017, **9**, 29363–29373.
63 Y. Miwa, J. Kurachi, Y. Kohbara and S. Kutsumizu, *Commun. Chem.*, 2018, **1**, 5.
64 C. Li, Z. Yuan and L. Ye, *Composites, Part A*, 2019, **126**, 105580.
65 J. Liu, C. Xiao, J. Tang, Y. Liu and J. Hua, *Ind. Eng. Chem. Res.*, 2020, **59**, 12755–12765.
66 A. M. Wemyss, A. Marathianos, E. L. Heeley, J. Ekeocha, Y. Morishita, R. di Ronza, M. M. Bernal, D. M. Haddleton and C. Wan, *ACS Appl. Polym. Mater.*, 2022, **4**, 7868–7877.
67 N. Lopattananon, A. Kraibut, R. Sangjan and M. Seadan, *J. Appl. Polym. Sci.*, 2007, **105**, 1444–1455.
68 Z. Yuan, W. Li, C. Li and L. Ye, *Composites, Part A*, 2019, **121**, 254–264.
69 L. Wang, Z. Hua and Z. Wang, *Polym. Test.*, 2019, **76**, 481–489.
70 Y. Liu, Z. Li, R. Liu, Z. Liang, J. Yang, R. Zhang, Z. Zhou and Y. Nie, *Ind. Eng. Chem. Res.*, 2019, **58**, 14848–14858.
71 N. F. M. Sani, N. L. N. Thajudin, N. Hayeemasae and R. K. Shub, *J. Appl. Polym. Sci.*, 2023, **140**, e53924.
72 J.-C. Lai, L. Li, D.-P. Wang, M.-H. Zhang, S.-R. Mo, X. Wang, K.-Y. Zeng, C.-H. Li, Q. Jiang, X.-Z. You and J.-L. Zuo, *Nat. Commun.*, 2018, **9**, 2725.
73 M. Salehi, K. Cornish, M. Bahmankar and M. R. Naghavi, *Ind. Crops Prod.*, 2021, **170**, 113667.
74 Y. Huang, Y. Liu, G. Si and C. Tan, *ACS Sustainable Chem. Eng.*, 2024, **12**, 2212–2224.
75 H. C. Kolb, M. G. Finn and K. B. Sharpless, *Angew. Chem., Int. Ed.*, 2001, **40**, 2004–2021.
76 G. B. Butler, *Ind. Eng. Chem. Prod. Res. Dev.*, 1980, **19**, 512–528.
77 B. Saville, *J. Chem. Soc. D*, 1971, 635–636.
78 K.-W. Leong and G. B. Butler, *J. Macromol. Sci., Chem.*, 1980, **14**, 287–319.
79 T. C. S. Chen and G. B. Butler, *J. Macromol. Sci., Chem.*, 1981, **16**, 757–768.
80 K. De Bruycker, S. Billiet, H. A. Houck, S. Chattopadhyay, J. M. Winne and F. E. Du Prez, *Chem. Rev.*, 2016, **116**, 3919–3947.
81 P. Mondal, P. K. Behera and N. K. Singha, *Prog. Polym. Sci.*, 2021, **113**, 101343.
82 L. Vlaminck, K. De Bruycker, O. Türünç and F. E. Du Prez, *Polym. Chem.*, 2016, **7**, 5655–5663.
83 H. Zhang, C. Ma, R. Sun, X. Liao, J. Wu and M. Xie, *Polymer*, 2019, **184**, 121904.
84 J. Zhao, H. Zhang, C. Ma, H. Han, R. Sun and M. Xie, *J. Polym. Sci., Part A: Polym. Chem.*, 2019, **57**, 1247–1255.
85 S. Fang, S. Wu, J. Huang, D. Wang, Z. Tang, B. Guo and L. Zhang, *Ind. Eng. Chem. Res.*, 2020, **59**, 21047–21057.
86 W. H. Pirkle and P. L. Gravel, *J. Org. Chem.*, 1978, **43**, 808–815.
87 A. Alberti and G. F. Pedulli, *J. Org. Chem.*, 1983, **48**, 2544–2549.
88 A. Nomura, J. Takano, A. Toyoda and T. Saito, *Nippon Gomu Kyokaishi*, 1993, **66**, 830–838.
89 Y. Nie, G. Huang, Z. Liu, L. Qu, P. Zhang, G. Weng and J. Wu, *J. Appl. Polym. Sci.*, 2010, **116**, 920–928.
90 R. Costin, W. Nagel and R. Ekwall, *Rubber Chem. Technol.*, 1991, **64**, 152–161.
91 Y. Lu, L. Liu, M. Tian, H. Geng and L. Zhang, *Eur. Polym. J.*, 2005, **41**, 589–598.
92 Y. Chen and C. Xu, *Polym. Compos.*, 2011, **32**, 1593–1600.
93 Y. Chen, C. Xu and Y. Wang, *J. Reinf. Plast. Compos.*, 2012, **31**, 705–716.
94 J. Chen, L. Liao, F. Zhang, S. Hu, J. Huang, S. Shen, D. He and M. Xue, *Polym. Eng. Sci.*, 2023, **63**, 1388–1400.
95 J. Chen, L. Liao, F. Zhang, T. Gao, L. Gao, L. Ma and X. Ma, *Polym. Eng. Sci.*, 2022, **62**, 1549–1561.
96 I. Pliskin and N. Tokita, *J. Appl. Polym. Sci.*, 1972, **16**, 473–492.
97 A. R. Payne, *J. Appl. Polym. Sci.*, 1965, **9**, 2273–2284.
98 S. Toki and B. S. Hisao, *Macromolecules*, 2003, **36**, 5915–5917.